Molecular Vision 2020; 26:76-90 <http://www.molvis.org/molvis/v26/76>
Received 22 May 2019 | Accepted 21 February 2020 | Published 25 February 2020

Cell senescence altered the miRNA expression profile in porcine angular aqueous plexus cells

Chen Tan,[1] Yiyan Yang,[2] Maomao Song,[1,3] Zhiwei Cao,[2] Xinghuai Sun,[1,3,4,5] Yuan Lei,[1,3] Junyi Chen[1,3]

(Last two authors contributed equally to this work.)

[1]Department of Ophthalmology & Visual Science, Eye & ENT Hospital, Shanghai Medical College, Fudan University, Shanghai, China; [2]Bioinformatics, School of Life Sciences and Biotechnology, Tongji University; [3]Key Laboratory of Myopia, NHFPC (Fudan University), Shanghai, China; [4]Shanghai Key Laboratory of Visual Impairment and Restoration (Fudan University), Shanghai, China; [5]State Key Laboratory of Medical Neurobiology, Institutes of Brain Science and Collaborative Innovation Center for Brain Science, Fudan University, Shanghai, China

Purpose: This study investigates the impact of aging on the miRNA expression profile in porcine angular aqueous plexus (AAP) cells, which are the porcine equivalent of human Schlemm's canal endothelial cells.
Methods: AAP endothelial cells were isolated and cultured in physiologic (5% O_2) or hyperoxic condition (40% O_2) for 14 days to induce cell senescence. miRNA and protein expression profiles of control and senescent cells were analyzed with miRNA microarray and isobaric tags for relative and absolute quantification (iTRAQ), respectively.
Results: The miRNA microarray identified 33 differentially expressed miRNAs in senescent cells compared with controls ($p<0.05$), and quantitative real-time PCR (qRT-PCR) confirmed 12 of them ($p<0.05$). iTRAQ analysis identified 148 upregulated and 222 downregulated proteins ($p<0.05$, fold change>1.2). Bioinformatics analysis of miRNA microarray and proteomics data predicted that six out of seven miRNAs are associated with aqueous humor outflow by targeting integrin and the downstream pathways (Src/Rho kinase, focal adhesion kinase (FAK)/NO-cGMP), and one miRNA might influence gap junction by targeting the Inositol trisphosphate receptor (IP3R) /Protein kinase C (PKC) pathway.
Conclusions: This study identified miRNAs in senescent AAP cells that might regulate aqueous humor outflow by targeting proteins involved in focal adhesion, cytoskeleton, NO-cGMP signaling, and gap junction.

Aging is a strong risk factor for developing primary open angle glaucoma (POAG) [1-7]. Schlemm's canal (SC) inner wall and juxtacanalicular tissue are the main sites of aqueous outflow resistance [8] which are responsible for the intraocular pressure (IOP) elevation in patients with POAG [8].

Senescence of SC and trabecular meshwork (TM) cells have been implicated in the initiation and progression of glaucoma [9-13]. The oxidizing species produced and accumulating during cell metabolism can cause molecular damage to the TM cells, which could increase aqueous humor outflow resistance [10,14]. Further, significantly higher levels of DNA oxidation products were observed in the TM of patients with glaucoma, and the level of DNA damage strongly correlated with IOP elevation and visual field defects [13,15].

Hyperoxia leading to senescence is an established model of aging which has been widely used in aging research [16-18]. This model has also been investigated in the cells of the outflow pathway in the context of glaucoma pathogenesis [10,14,19,20]. This model is based on one of the most accepted theories of aging, stress-induced premature senescence (SIPS) [21]. This model provides a constant increase in reactive oxygen species without the need for additional chemical or cellular treatments and has relatively low toxicity in that sustained confluence, and thus, normal post-mitotic conditions were assured throughout the length of the experiment [22-24].

Our previous studies showed that cell senescence influenced cell monolayer permeability through cytoskeletal proteins and cell adhesion proteins in porcine angular aqueous plexus (AAP) cells [25]. Moreover, we demonstrated that senescence reduced the mechanotransduction sensitivity of AAP cells; specifically, the senescent cells were less able to respond to shear stress which should downregulate junctional proteins to facilitate aqueous humor drainage and maintain IOP homeostasis [12]. Cell senescence also altered eNOS and phosphorylated eNOS, and resulted in reduced NO production [26]. However, the mechanism by which these responses were regulated remains unknown.

MicroRNAs (miRNAs) are highly conserved non-coding RNAs. They typically negatively regulate protein expression [27] by binding to their target sites in the 3′-untranslated region (UTR) of the mRNA. miRNAs are key modulators of cellular senescence. miRNAs are differentially expressed in

Correspondence to: Junyi Chen, Department of Ophthalmology, 83 Fenyang Road, Shanghai, China; email: chenjy@fudan.edu.cn

senescent cells, which further implicates them in the implementation of the senescent phenotype [28-30]. The dysregulation of miRNA-governed senescence underlies age-associated diseases [31-33] and cancer [34]. Researchers reported the miRNA profile in the aqueous humor of patients with glaucoma and identified several differentially expressed miRNAs [35-37]. Further, microRNAs were differentially expressed in the retinas of eyes with advanced glaucomatous damage compared with normal controls [38]. This evidence suggests that miRNA may be important in the pathogenesis of glaucoma and merits further investigation. However, the miRNA expression profile is not known in senescent Schlemm's canal endothelial cells.

This study aimed to characterize miRNA expression profile in senescent AAP cells, which are the porcine equivalent of human SC cells. These results were further correlated to the protein expression profile with isobaric tags for relative and absolute quantification (iTRAQ) analysis to identify their target proteins. Bioinformatics analysis revealed the differentially expressed miRNAs may regulate critical pathways involved in aqueous humor outflow.

METHODS

Experimental design: This study adhered to the ARVO Statement for Use of Animals in Research. And our research was proved by Laboratory Animal Management and Ethic Committee of Eye & ENT Hospital. Porcine AAP cells were isolated and cultured. Cell senescence was induced by hyperoxia for 2 weeks. miRNA microarray and proteomics analyses of normal and senescent AAP cells were performed to identify differential miRNAs and proteins. miRNA and protein data were correlated with bioinformatics analysis. The workflow of this study is shown in Figure 1.

Cell culture: Cell culture AAP endothelial cells were isolated, cultured, and characterized according to an established method [39]. Briefly, for each cell line, outflow tissue from ten porcine eyes (4- to 6-month-old pigs) was collected. The cells were allowed to multiply for 8 days and then treated with puromycin (4 µg/ml, InvivoGen, San Diego, CA) for 2 days. The puromycin-selected cells were similar to human Schlemm's canal endothelial cells in that the cells exhibited contact inhibition and expressed the same surface markers as those seen in cultured human SC cells and whole porcine tissue (Appendix 1). Three independent cell lines (each cell line came from ten porcine eyes) were used as one biological replicate for microarray assay or iTRAQ analysis.

Cell senescence model: Cell senescence was induced by a model of chronic oxidative stress [20,25]. Cells were cultured under normobaric hyperoxia condition (40% O_2, 5% CO_2) for 14 days in a triple-gas incubator (Smart cell, Shanghai, China). Control cultures were grown under physiologic oxygen condition (20% O_2, 5%CO_2) for 14 days in parallel with the experimental group of the same cell line. AAP cells were stained positive for endothelial cell specific markers VE-cadherin and eNOS, and senescence of AAP cells was confirmed with β-galactosidase staining (Appendix 1). The expression levels of p53 and p21 and cell cycle analysis were also investigated to ensure cell senescence (Appendix 1).

MicroRNA microarray assay: The miRNA microarray analysis was performed three times using three independent cell samples (each individual cell line came from ten porcine eyes). Total RNA was isolated with an miRNeasy kit (QIAGEN, Shanghai, China). The RNA integrity number (RIN) was assessed using a Bioanalyzer (Agilent 2100, Shanghai, China) according to the manufacturer's instructions. It allows visual inspection of RNA integrity to determine the RNA quality. Only samples that achieved an RIN score greater than 9.5 were used for further microarray analysis. The miRNA

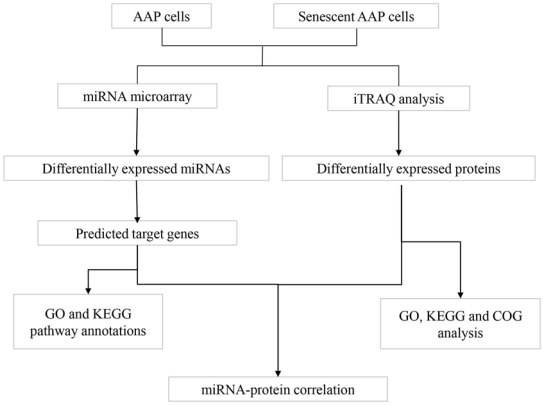

Figure 1. Experimental design and work flow. After the microarray and proteomics analysis of normal and senescent aqueous plexus (AAP) cells, bioinformatics analysis was performed to determine key Gene Ontology (GO) and Kyoto Encyclopedia of Genes and Genomes (KEGG) pathways, and miRNA-protein correlations.

microarray analysis was performed three times. In each one of the biological replicates, miRNA expression was measured using eight technical replicates.

The miRNA microarray analyses were performed using different samples by LC Sciences (Houston, TX). (The sequences are listed in Appendix 2) Four to eight micrograms of total RNA samples were fluorescence labeled and hybridized overnight. Fluorescence signals were collected using a laser scanner (GenePix 4000B, Molecular Devices, San Jose, CA) and digitized (Array-Pro, Media Cybernetics, Rockville, MD). After the background signals were subtracted, data were normalized using a locally weighted scatterplot smoothing (LOWESS) filter, which is a preferred method for miRNA data sets [40]. Signals between groups were compared with the Student *t* test. To include as many miRNA candidates as possible, a p value of less than 0.05 without fold-change limitation was regarded as statistically significant.

Quantitative real-time PCR: Quantitative real-time PCR (qRT-PCR) of differentially expressed miRNAs was performed using qTOWER 2.2 (Analytik Jena, Jena, Germany) to validate differentially expressed miRNAs ($p<0.05$) to ensure statistical significance. RNA was extracted from three experimental samples and three control samples which were different from those used in the microarray analysis. cDNAs were synthesized in 40 µl reaction volume. The primer sequences are listed in Appendix 3. Amplification and detection were performed on 96-well plates. Each 10 µl Bestar™Real time PCR Master Mix (DBI, München, Germany) contained 5 µl 2×SYBR® Green Supermix, 1 µl cDNA reaction mixture, 0.5 µl reverse and sense primers, as well as 3 µl distilled deionized water (ddH_2O). The reaction conditions were as follows: initial denaturation at 95 °C for 3 min, followed by 40 cycles of 95 °C for 10 s, 58 °C for 30 s, and finally 60 °C~95 °C,+1 °C/cycle holding time 4 s for melting curve analysis. The expression levels of mRNA were normalized to reference genes U6. Relative miRNA levels were calculated using the Pfaffl method [41] with the installed software qPCRsoft3.0. (The Pfaffl method is preferred for large differences between the amplification efficiency of the target gene and the internal gene.)

iTRAQ: iTRAQ technology is a widely used method in the field of quantitative proteomics with high accuracy and reliability. It is an isobaric labeling method by tandem mass spectrometry to determine the number of proteins from different sources in a single experiment [42,43]. Proteomics of control cells and senescent cells were performed with iTRAQ, which detected the whole proteome in porcine proteins. iTRAQ analysis was performed three times.

Cell lysates were processed with radioimmunoprecipitation assay (RIPA) solution. Then, the protein concentration was measured using the Bradford method. One hundred micrograms of protein from each sample was processed for iTRAQ labeling. Then, the proteins were denatured, reduced, alkylated, trypsin digested, and labeled with iTRAQ labeling (8-plex iTRAQ, AB SCIEX, Framingham, MA). The pooled iTRAQ-labeled peptides were fractionated with strong cation exchange (SCX) chromatography (Shimadzu LC-20AB HPLC Pump system) using an SCX column containing 5 mm particles (4.66250 mm Ultremex column, Phenomenex, Torrance, CA).

The eluted peptides were pooled as 20 fractions, desalted with the Strata X C18 column (Phenomenex), and vacuum-dried. The elute from the Nano Liquid Chromatography system (Shimadzu LC-20AD) was coupled to a tandem mass spectrometer in an LTQ Orbitrap Velos (ThermoFisher Scientific, San Jose, CA), through an electrospray ionization source equipped with a 15 µm ID emitter tip.

Similar to previous publications ([44,45]), protein expression ratios of >1.2 or <0.83 and a p value of less than 0.05 according to the Student *t* test were considered differential proteins. The abundance ratio was calculated using the unique peptide strength corresponding to each protein (the sum of the ion strength of the identification spectrum label) to calculate the average ratio. Protein coverage is the length of the sequence identified in the protein divided by the length of the total protein sequence. If the unique peptide segment identified in the protein met the false discovery rate (FDR) filtering criteria, the protein was identified. Complete experimental details for iTRAQ are in Appendix 4.

Bioinformatics analysis: Differentially expressed miRNAs of the control and experimental groups were identified with the *t* test using TMev bioinformatics software. To get the gene targets of differentially expressed miRNAs, porcine 3′-UTR sequences of mRNA were downloaded from the Ensemble database and complementarily linked with miRNA sequences. The final predicted targets and their corresponding proteins were determined by the intersection of results from three different databases (TargetScan, PicTa, and miRanda), which makes the prediction more reliable and highly accurate. Clustering analysis was routinely performed using the hierarchical method when the p value was less than 0.01. Average linkage and Euclidean distance metric were performed in cluster analysis. Gene Ontology (GO) and Kyoto Encyclopedia of Genes and Genomes (KEGG) pathway annotations were performed against porcine proteins using the DAVID gene annotation tool.

Bioinformatics analysis on the raw tandem mass spectrometry (MS/MS) data was performed according to a standard protocol (Appendix 4). Taking the amino acid sequences as input, differentially expressed proteins (iTRAQ) were further annotated with GO and Cluster of Orthologous Groups (COG) analysis. GO functional classifications were analyzed with Blast2GO software, while COG information was retrieved by blasting the sequences on the COG database [46]. To explore the biological meanings of these proteins, GO enrichment analysis was performed to identify GO terms that were statistically significantly enriched in differentially expressed proteins ($p<0.05$), and the enriched metabolic pathways of these identified proteins were screened via the KEGG database ($p<0.05$).

Target proteins of differentially expressed miRNAs were identified from the iTRAQ analysis. These differentially expressed proteins were further mapped to KEGG pathways, if more than three proteins are related to known pathways that are important to the pathogenesis of glaucoma.

Western blotting: Cell lysates were prepared according standard protocols. Briefly, cells were prepared using RIPA solution. After protein concentrations were measured with the Bradford method, equal amounts of protein (30 µg protein/lane) were separated with 10% sodium dodecyl sulfate–polyacrylamide gel electrophoresis (SDS-PAGE). Then the resolved proteins were transferred to nitrocellulose filters which was then blocked with 5% nonfat dry milk in Tris-buffered saline with 0.05% Tween-20 for 2 h. Filters were probed using primary antibodies, ITGAV (1:1,000, Abcam), ITGB3 (1:1,000, Abcam) pMLC (1:1,000), sGC (1:3,000), and eNOS (1:1,000), followed by incubation with peroxidase-linked secondary antibodies. GAPDH was used as a loading control. Four independent replicates were used for statistical analysis with the Student *t* test.

RESULTS

Differential microRNA expression in senescent AAP cells: We identified differentially expressed miRNAs in senescent AAP cells with miRNA microarray analysis. Among the 407 miRNAs identified, 102 miRNAs were statistically significantly expressed in senescent cells compared to controls ($p<0.05$). The microarray raw data are shown in Appendix 5. The miRNA microarray hybrid signal ranged from 0 to 51,949; those that had a value greater than 500 were further analyzed (in our experience, a low hybrid signal was more likely to result in false positives). The heat map of the miRNAs shown in Figure 2 demonstrated 17 statistically significantly downregulated miRNAs and 16 statistically significantly upregulated miRNAs ($p<0.05$, signal>500, n=3, Student *t* test; detailed information is listed in Appendix 6). Then differential miRNAs were validated with qRT-PCR, which confirmed 12 miRNAs (Table 1).

Target genes and proteins of differentially expressed miRNAs are listed in Appendix 7. GO analysis revealed 504 GO terms with p values smaller than 0.05 with the submission of predicted target genes. GO terms of top-ranked classification gene numbers are listed in Appendix 8. Some are relevant to aqueous outflow, for example, extracellular matrix organization (GO:0030198, p=0.0111, gene number: 33), cell–cell junction organization (GO:0045216, p=0.0095, gene number: 10), focal adhesion (GO:0005925, p<0.0001, gene number: 139), cytoskeleton (GO:0005856, p=0.0056, gene number: 88), cell–cell junction (GO:0005911, p=0.0043, gene number: 65), microtubule cytoskeleton (GO:0015630, p=0.0436, gene number: 52), adherents junction (GO:0005912, p=0.0268, gene number: 14), and actin binding (GO:0003779, p=0.0316, gene number: 92).

KEGG analysis identified 138 pathways with p values smaller than 0.05. The top 20 KEGG pathways ranked by predicted gene number are listed in Appendix 8. Some are possibly involved in aqueous humor drainage.

Differential protein expression in senescent AAP cells: iTRAQ analysis identified a total of 4,165 proteins and 17,603 unique peptides. The top ten up- and down-expressed proteins are presented in Table 2, and raw data are shown in Appendix 9 and Appendix 10. The protein abundance distribution is shown in Appendix 11. A total of 370 proteins were differentially expressed ($p<0.05$, fold change>1.2 or <0.83), of which 148 proteins were upregulated, and 222 proteins were downregulated. Protein fold-difference was expressed in log form with the base equaling 2. A log ratio greater than 0 indicates upregulation; less than 0 is downregulation. Most of the values fell within −5 and 5 (Figure 3). GO classification and enrichment analysis revealed the functional groups of differentially expressed proteins (Figure 4, Appendix 8). Intermediate filament (2.0%), extracellular matrix (3.8%), and cell–cell contact zone (1.5%) were identified. The KEGG pathway enrichment analysis is shown in Appendix 8. The COG protein analysis showed the protein distribution in different cell functional groups (Figure 5).

Identification of miRNA and protein pairs: Differentially expressed miRNA and protein pairs are presented in Table 3. A total of seven miRNAs and 13 proteins were further mapped to KEGG pathways after selection. These miRNAs were computationally predicted to negatively or positively regulate their target proteins (Figure 6). Six miRNAs were predicted to directly target ITGA/ITGB, the two subunits of integrin, which could regulate IOP through the downstream

pathways related to focal adhesion, cytoskeleton, NO-cGMP, and gap junction. Western blot (WB) verification of ITGAV and ITGB3 show no statistically significant changes in Figure 7. The possible reasons are analyzed in the Discussion section. However, the proteins (pMLC, eNOS, and sGC) of the downstream pathways showed a statistically significant difference.

DISCUSSION

This study identified a range of differentially expressed miRNAs and proteins in senescent AAP cells, which are the porcine equivalent of SC cells. The senescence of SC cells was thought to contribute to the elevation of IOP [11,12]. By correlating the miRNA microarray data with proteomics data, we identified those key miRNAs whose target proteins are also statistically significantly altered in AAP cells. The integration and analysis of differential miRNA and proteomics

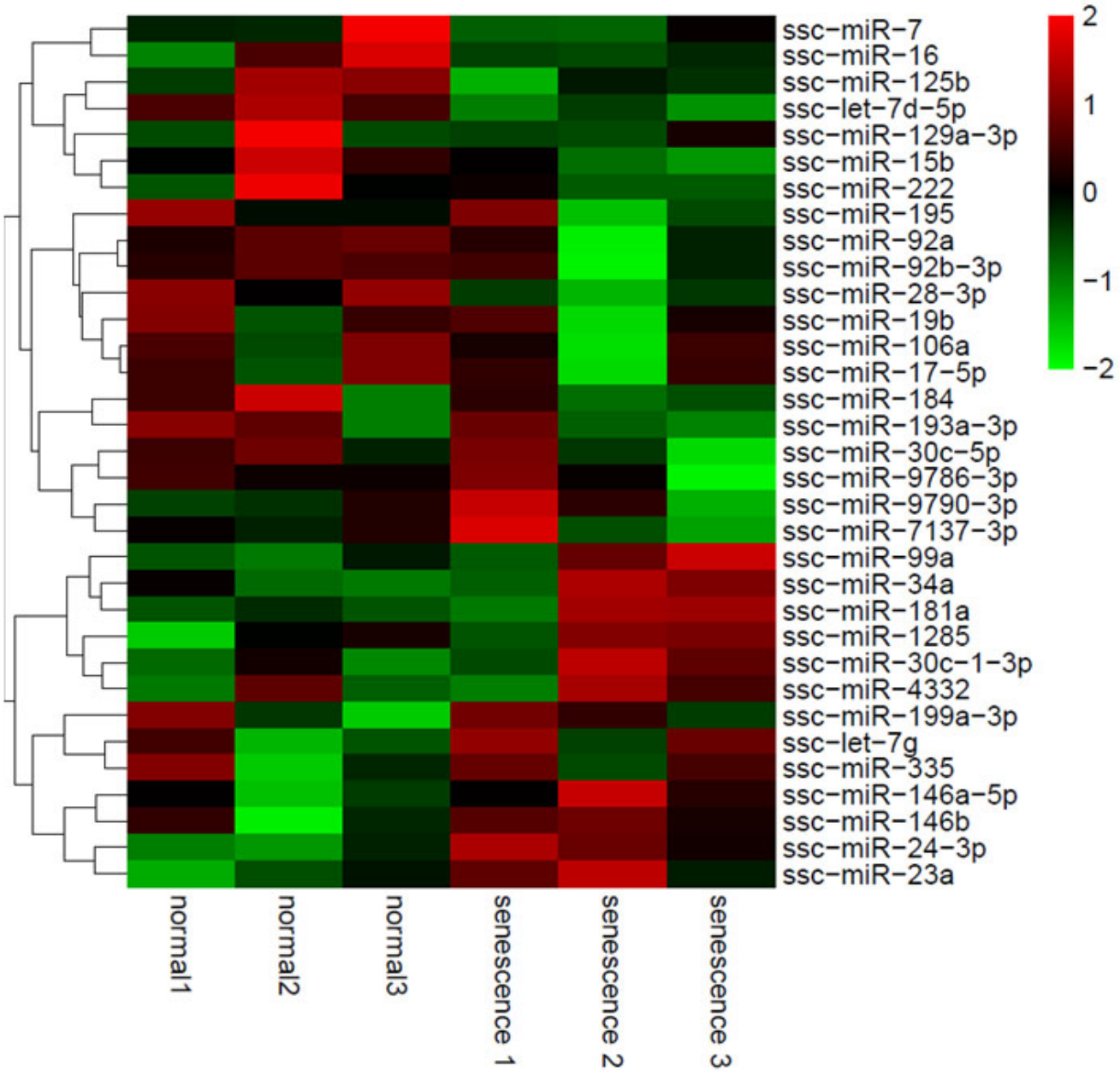

Figure 2. miRNA expression in APP cells. Heat map of miRNAs ($p<0.05$, signal>500, n=3, Student *t* test). Seventeen miRNAs were statistically significantly downregulated and 16 miRNAs significantly upregulated.

Table 1. Differentially expressed miRNAs by qPCR validation.

miRNA	P value	Fold change	Up/downregulated
ssc-miR-146a-5p	0.0000	3.5546	Up
ssc-miR-146b	0.0000	2.5848	Up
ssc-miR-34a	0.0000	1.6304	Up
ssc-miR-99a	0.0005	1.5362	Up
ssc-miR-24–3p	0.0000	1.4731	Up
ssc-miR-181a	0.0001	1.3115	Up
ssc-miR-23a	0.0207	1.1387	Up
ssc-let-7g	0.0018	1.1241	Up
ssc-let-7d-5p	0.0129	0.9136	Down
ssc-miR-15b	0.0000	0.4996	Down
ssc-miR-129a-3p	0.0463	0.3948	Down
ssc-miR-184	0.0000	0.0590	Down

Fold changes were calculated from the normalized signal ratio of the senescent AAP cells over normal AAP cells. P values were obtained by Student *t* test (n=3).

data may help us to better understand the responses occurring in SC cells under senescence.

miRNA microarray analysis identified 33 differentially expressed miRNAs (Appendix 6). However, the results of the miRNA microarray assays presented an inconsistent pattern within groups. Our speculation is that the difference between primary cells might be the possible reason for the inconsistency within groups. Although the variation is large, which may lead to omission, the detected miRNAs were unaffected. In addition, these miRNAs were confirmed with

Table 2. Top 10 differentially expressed proteins by iTRAQ.

Ensembl annotation	Gene alias	Fold change	Up/downregulated
ENSSSCP00000011355	PNLIP	5.523	Up
ENSSSCP00000005754	ALDH1B1	5.469	Up
ENSSSCP00000024109	CTRB2	4.479	Up
ENSSSCP00000016408	CHI3L1	4.422	Up
ENSSSCP00000027363	C3	3.773	Up
ENSSSCP00000020422	CLIC4	3.483	Up
ENSSSCP00000011244	SCD	3.38	Up
ENSSSCP00000025323	TFF2	3.117	Up
ENSSSCP00000000251	KRT75	3.005	Up
ENSSSCP00000004526	ENPP1	2.966	Up
ENSSSCP00000010111	KCTD12	0.116	Down
ENSSSCP00000011028	PRXL2A	0.189	Down
ENSSSCP00000006775	APOA2	0.232	Down
ENSSSCP00000009695	FGF2	0.236	Down
ENSSSCP00000017259	GIGYF2	0.241	Down
ENSSSCP00000027528	HMOX1	0.248	Down
ENSSSCP00000023743	COTL1	0.295	Down
ENSSSCP00000024753	NUDCD2	0.34	Down
ENSSSCP00000027850	ARSA	0.352	Down
ENSSSCP00000025799	NXF1	0.377	Down

PCR to ensure a statistically significant difference. Twelve were verified with PCR. All 12 miRNAs were previously found to be altered or participate in cell senescence. Three miRNAs (miR-146a [47], miR-146b, and miR-15b [30]) were also detected in senescent TM cells. The other nine miRNAs (miR-34a [48], miR-99a [49], miR-24–3p [50], miR-181a [51], miR-23a [52], let-7g [53], let-7d-5p [54], miR-129a-3p [55], and miR-184 [56]) were also found to be involved in senescence in other cell types.

The total differential expressed miRNAs produced a total of 504 GO terms and 138 KEGG pathways. Some were identified to regulate IOP by actin binding, cytoskeleton, actin binding, cell–cell junction, extracellular matrix (ECM) organization, focal adhesion, and so on. In SC cells, stiffness [57] and junctions are related to the formation of pores. Reorganization of extracellular matrix [59] alters basement membrane permeability. The present findings are consistent with those of previous studies. For example, the let-7 family is believed to inhibit fibrosis by repressing expression of collagen genes [60]. miR-24-3p accelerated the migration and invasion of bladder cancer cells [61]. miR-15b directly targets tissue inhibitor of metallopeptidases 2 (TIMP2) to increase the migration and invasion of human lung cancer cells [62]. However, overexpression of miR-15b aggravates IL-1beta-induced ECM degradation [63] in nucleus pulpous cells. In other words, these miRNAs were found to be involved in ECM regulation and cell junctions. The differential expression of 12 miRNAs was confirmed with PCR (Table 1). miRNA-protein pairs were identified for these miRNAs. A total of 4,165 proteins and 17,603 unique peptides were identified. GO and COG protein analysis further classified these differential proteins according to their functions. Binding, catalytic activity, and transporter activity were included in top molecular functions. The top biological processes were the cellular process, metabolic process, and single-organism process. In senescent cells, these top changes in molecular function and biological processes were reasonable and consistent with the cellular senescence hallmark [64,65]. In the senescent endothelial cells, signaling, biological adhesion, and localization might relate to alteration of the endothelial cell barrier and interaction with ECM.

Bioinformatic analysis further revealed that the seven miRNAs might regulate aqueous humor outflow in AAP cells through three signaling pathways which are important to glaucoma pathogenesis (Figure 6). The three pathways form a network through integrin and PKG. In the following, we discuss each signaling pathway in detail.

First, miR-23a, miR-146a-5p, miR-146b, and let-7g could regulate aqueous humor outflow by integrin/Src/Rho kinase/MLC/F-actin. ITGA and ITGB are direct targets of miR-23a, miR-146a-5p, miR-146b, and let-7g. Upon engagement of integrin receptors with extracellular ligands, the focal adhesion kinase (FAK)-Src complex is activated. Src transiently inhibits RhoA activity through RhoGAP and GRLF1 (p190RhoGAP) [66,67]. RhoA and Rac stimulation can increase the transendothelial resistance of human SC cells, by phosphorylating MLC [68], and MLC phosphorylation can trigger F-actin organization which impacts focal adhesion and cell permeability [69]. It has also been reported that Rho-associated protein kinase inhibitor significantly decreases outflow facility by targeting junction or calcium ion transport of SC cells [70,71]. Rho kinase and MLC are important pharmaceutical targets for ocular hypertension. Rho kinase inhibitor (netarsudil, NDA:208254) was recently approved by the U.S. Food and Drug Administration (FDA)

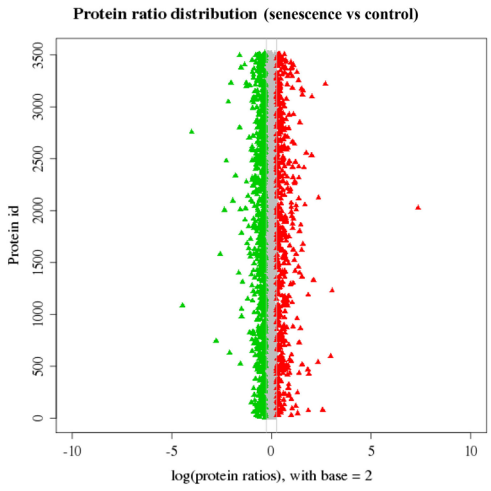

Figure 3. Protein abundance ratio distribution. Differentially expressed proteins ($p<0.05$, fold change>1.2 or <0.83, n=3, Student *t* test) are plotted in this scattergram. A total of 148 upregulated proteins and 222 downregulated proteins were observed.

as a novel glaucoma drug to increase conventional outflow and treat ocular hypertension. MLC kinase inhibitor is also a potential new therapy for lowering IOP [72]. It might be possible to use their upstream miRNA to regulate outflow through Rho kinase and MLC.

Second, let-7d-5p and miR-184 could regulate outflow by integrin, FAK, PI3K, Akt, eNOS, and NO-cGMP. The activation of ITGA and ITGB phosphorylates FAK, which is upstream of the phosphatidylinositol 3-kinase (PI3K)/Akt signal pathway [73]. In a previous study, we showed that PI3K/Akt facilitates aqueous humor drainage through activation of eNOS [74], an enzyme that catalyzes the release of NO [75]. NO-cGMP is an important pathway for IOP regulation. The NO-donating prostaglandin analog latanoprostene bunod (LBN) was developed as a novel drug for ocular hypertension [76].

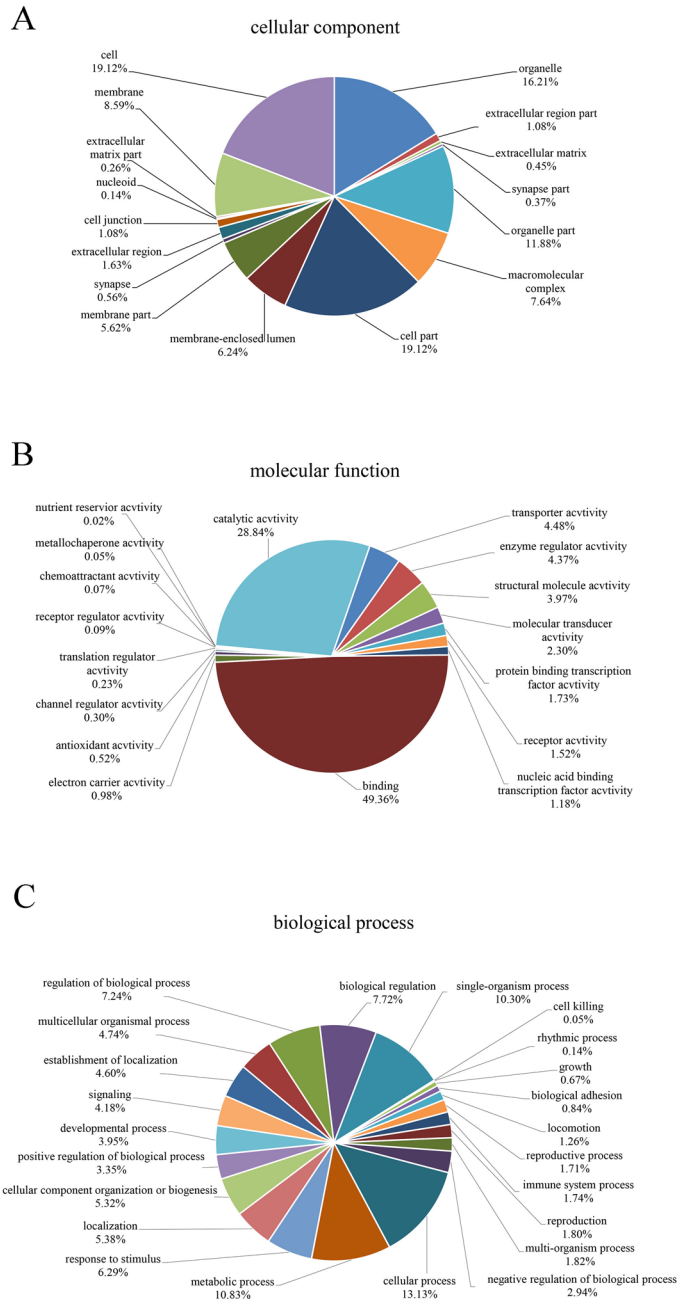

Figure 4. GO analysis of identified proteins with the iTRAQ method. Gene Ontology includes the cellular component (**A**), molecular function (**B**), and biological process (**C**). Cell junction and extracellular matrix proteins are closely related to intraocular pressure (IOP) regulation (**A**). Molecular function such as binding, catalytic activity, transduction, and antioxidant activity are all implicated in IOP regulation (**B**). Biological adhesion is also key to IOP regulation (**C**).

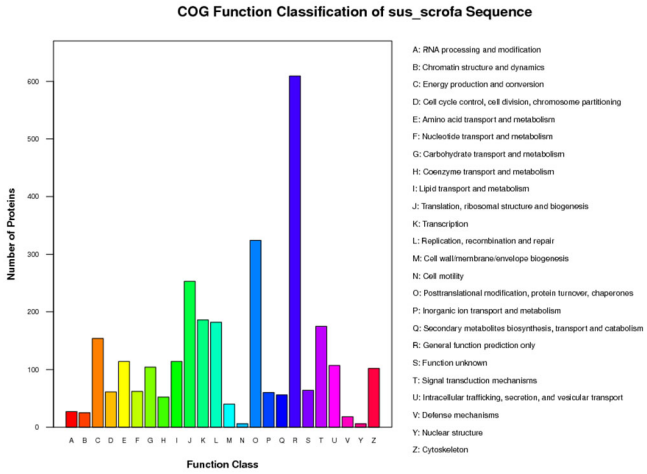

Figure 5. COG analysis of differentially expressed proteins. Among the 24 terms, the top three protein function classes are general function prediction only, posttranslational modification, protein turnover, chaperones, and translation, ribosomal structure, and biogenesis.

Third, miR-24–3p could regulate aqueous humor outflow by IP3R, Ca^{2+}, and PKC which indirectly controls gap junction. Gap junction is related to endothelial cell stiffness [77], which may affect IOP homeostasis potentially by vacuole and pore formation in SC cells [57,77]. Gap junction blocker (e.g., carbenoxolone) significantly increases outflow facility [58]. Activation of IP3R by miR-24–3p results in the release of Ca^{2+} from the endoplasmic reticulum (ER) [78]. The increase in the Ca^{2+} concentration activates connexins, a family of transmembrane proteins that constitute the gap junction channels

Table 3. miRNA-target genes pairs.

MiRNA ID	Up/down (miRNA)	Target gene	Up/down (protein)	Regulation type
ssc-let-7d-5p	Down	SCD, ITGB3, KRT5, NAP1L1, ACSS2	Up	Negative
		RANBP2, FNDC3B, IGF2BP2	Down	Positive
ssc-let-7g	Up	RANBP2, FNDC3B, IGF2BP2	Down	Negative
		SCD, ITGB3, KRT5, NAP1L1, ACSS2	Up	Positive
ssc-miR-129a-3p	Down	WDR26, TM9SF3, SBDS	Up	Negative
ssc-miR-146a-5p	Up	ITGAV, NAP1L1, VBP1, VPS36	Up	Positive
ssc-miR-146b	Up	ITGAV, NAP1L1, VBP1, VPS36	Up	Positive
ssc-miR-15b	Down	SCD, CALU, ARL1, NEK9, ACSS2, CAB39, SBDS	Up	Negative
		ACSL4, TRPA1, SNRPA1, RRM1, GRK5, FNDC3B	Down	Positive
ssc-miR-181a	Up	FNDC3B, IGF2BP2	Down	Negative
		SCD, ENPP1, HSD11B1, PSME4, NEK9, TM9SF3	Up	Positive
ssc-miR-184	Down	ITGB3, HADH	Up	Negative
		EPHX1, GYS1	Down	Positive
ssc-miR-23a	Up	SKIV2L2, SF3A1	Down	Negative
		ITGAV, TM9SF3	Up	Positive
ssc-miR-24–3p	Up	GRK5, SKIV2L2, PARK7, DDX18, CYB5R1	Down	Negative
		RPL35, RAB5C, ITPR3, NEK9	Up	Positive
ssc-miR-34a	Up	ACSL4, SF3A1, TM9SF4	Down	Negative
		JUP, ALCAM	Up	Positive

[79]. Connexin phosphorylation can change the unitary conductance and open probability of gap junctions [80].

It is interesting that six out of seven miRNAs directly target integrin and the expression of integrin. Integrin is a transmembrane heterodimer with two subunits (α and β). It serves as a ligand binding site with various downstream signaling in cytoplasmic side [81]. Integrin is the binding site for structural adaptors (e.g., talin and tensin) which link directly to cytoskeleton [82]. Integrin is also the binding site for scaffolding adaptors (e.g., kindlin and paxillin) which contribute to focal adhesion [83]. As the binding site for catalytic adaptors, integrin interacts with Src and FAK which act as a signal transducer from adhesion molecules [84]. ECM proteins are the primary ligands for integrin; integrin activation can enhance ECM deposition by integrin-mediated matrix assembly and therefore increase aqueous humor outflow resistance. However, an agonist of the integrin subtype α4β1 could increase cell–ECM detachment in SC cells and increase outflow facility [85].

In the present study and our previous study, although the downstream expression levels of proteins (pMLC, eNOS, and sGC) and cellular functions [11,12,26] were validated to be altered, the levels of ITGAV and ITGB3 were not statistically significantly changed, accompanied by the increased expression of some miRNAs (miR-23a, 146a-5p, miR-146b, and let-7g) and the decreased expression of some miRNAs (let-7d-5p and miR-184). As the pathway showed, the ITGAV and ITGB3 expression levels depended on the integrated results of multiple regulation. Therefore, the combined effect was hard to define when not only upregulated miRNAs were considered. As the accumulated effect of miRNAs on integrin in the present study remains elusive, further studies are needed to improve our understanding of the associations between these miRNAs and integrin. A limitation of this study is that it did not validate the effect of the miRNAs

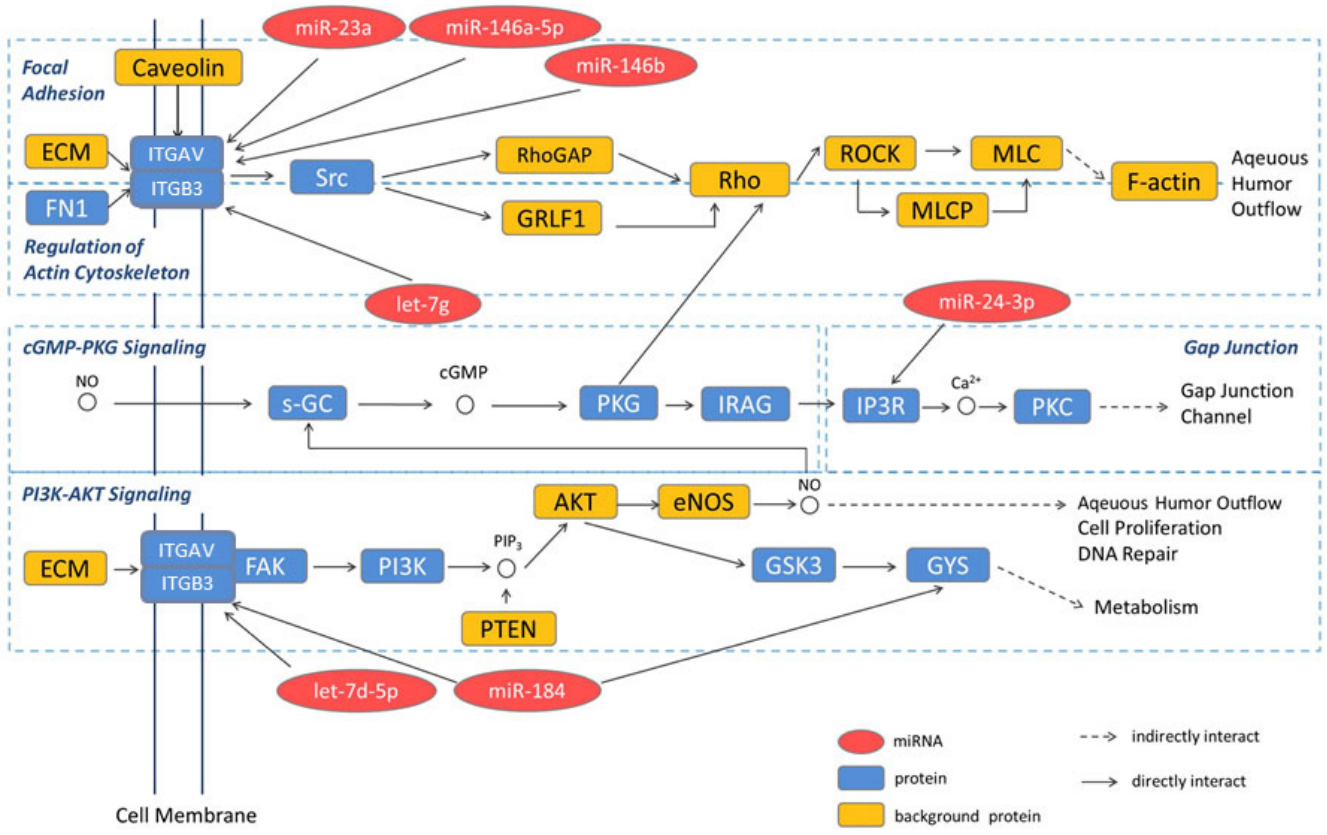

Figure 6. Correlation of miRNA and its corresponding regulated target proteins based on the KEGG database. Six miRNAs were predicted to directly interact with cell membrane protein integrin and influence aqueous humor by Src/Rho kinase and the Focal Adhesion Kinase (FAK)/Nitric Oxide-Cyclic Guanosine (NO-cGMP) pathway. One miRNA might affect gap junction channel through the Inositol trisphosphate receptor (IP3R)/Protein kinase C (PKC) pathway.

on aqueous humor outflow function, and this might be done in future studies. In conclusion, this study identified seven differentially expressed miRNAs in senescent AAP cells, which could contribute to IOP elevation by regulating three pathways responsible for cytoskeleton, focal adhesion, NO-cGMP signaling, and gap junction.

APPENDIX 1. CELL CHARACTERIZATION OF NORMAL AND SENESCENT AAP CELLS.

To access the data, click or select the words "Appendix 1."

APPENDIX 2. MICROARRAY LAYOUT.

To access the data, click or select the words "Appendix 2."

APPENDIX 3. QRT-PCR PRIMER SEQUENCES.

To access the data, click or select the words "Appendix 3."

APPENDIX 4. ITRAQ METHOD IN DETAIL.

To access the data, click or select the words "Appendix 4."

APPENDIX 5. MICROARRAY RAW DATA.

To access the data, click or select the words "Appendix 5."

APPENDIX 6. DIFFERENTIALLY EXPRESSED MIRNAS.

To access the data, click or select the words "Appendix 6."

APPENDIX 7. TARGET PREDICTION.

To access the data, click or select the words "Appendix 7."

APPENDIX 8. BIOINFORMATICS ANNOTATIONS.

To access the data, click or select the words "Appendix 8."

APPENDIX 9. UPREGULATED PROTEINS BY ITRAQ ANALYSIS.

To access the data, click or select the words "Appendix 9."

APPENDIX 10. DOWNREGULATED PROTEINS BY ITRAQ ANALYSIS.

To access the data, click or select the words "Appendix 10."

APPENDIX 11. PROTEIN DISTRIBUTION.

To access the data, click or select the words "Appendix 11."

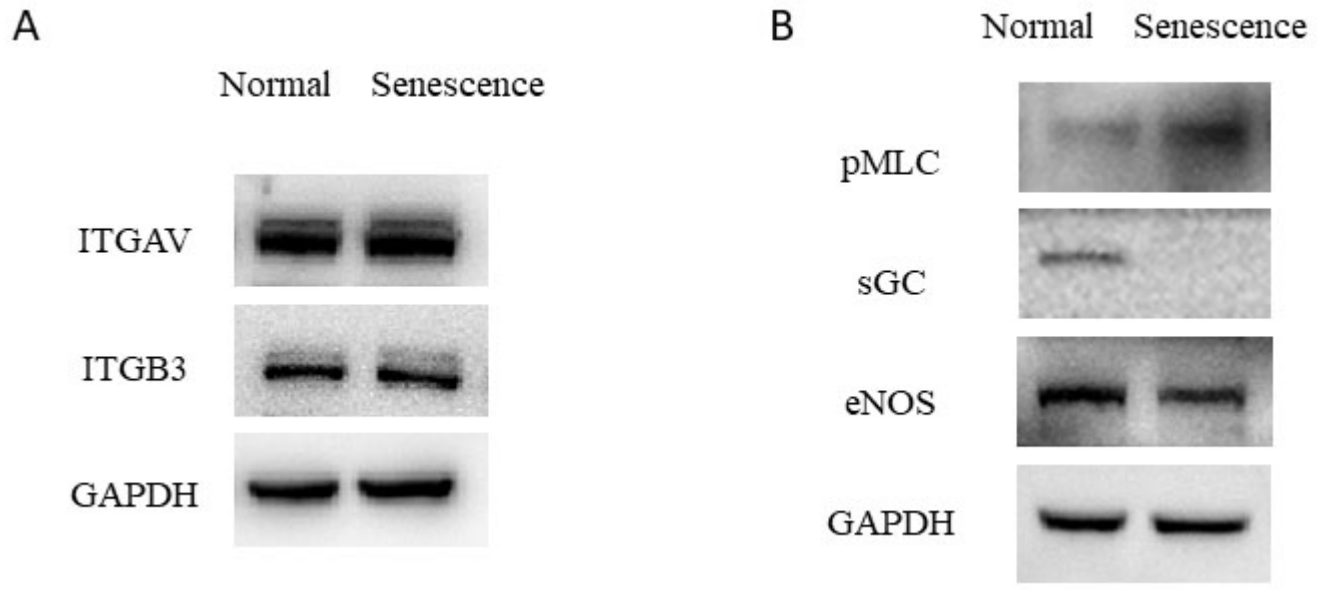

Figure 7. Expression validation of proteins in the predicted pathways. Representative blot images of pathway proteins are shown. ITGAV and ITGB3 were not statistically changed in senescent aqueous plexus (AAP) cells (ITGAV p=0.67, ITGB3 p=0.19, n=4, Student *t* test), but ITGB3 showed a trend of higher level (**A**, **B**). pMLC, eNOS, and sGC showed statistically significant changes in this pathway ($p<0.05$, n=3, Student *t* test).

ACKNOWLEDGMENTS

This research was founded by State Key Program of National Natural Science Foundation of China (81430007), General Program of National Science Foundation China (81100662, 81371015, 81870661, 81470623), 211 Project of Fudan University (EHF158351), Young scientists program of EENT Hospital of Fudan University and BrightFocus Foundation (G2018112). Prof. Yuan Lei (lilian0167@hotmail.com) and Prof. Junyi Chen (chenjy@fudan.edu.cn) contributed equally to this research, and were regarded as co-corresponding authors.

REFERENCES

1. Friedman DS. Prevalence of Open-Angle Glaucoma among Adults in the United States. Arch Ophthalmol 2004; 122:532-8. [PMID: 15078671].
2. Repka MX, Quigley HA. The effect of age on normal human optic nerve fiber number and diameter. Ophthalmology 1989; 96:26-32. [PMID: 2919049].
3. Drance S, Anderson DR, Schulzer M. Risk factors for progression of visual field abnormalities in normal-tension glaucoma. Am J Ophthalmol 2001; 131:699-708. [PMID: 11384564].
4. Mason RP, Kosoko O, Wilson MR, Martone JF, Cowan CL Jr, Gear JC, Ross-Degnan D. National survey of the prevalence and risk factors of glaucoma in St. Lucia, West Indies. Part I. Prevalence findings. Ophthalmology 1989; 96:1363-8. [PMID: 2789357].
5. Leske MC, Connell AM, Schachat AP, Hyman L. The Barbados Eye Study. Prevalence of open angle glaucoma. Arch Ophthalmol 1994; 112:821-9. .
6. Wensor MD, McCarty CA, Stanislavsky YL, Livingston PM, Taylor HR. The prevalence of glaucoma in the Melbourne Visual Impairment Project. Ophthalmology 1998; 105:733-9. [PMID: 9544649].
7. Tielsch JM, Sommer A, Katz J, Royall RM, Quigley HA, Javitt J. Racial variations in the prevalence of primary open-angle glaucoma: The Baltimore eye survey. JAMA 1991; 266:369-74. [PMID: 2056646].
8. Ethier CR, Read AT, Chan D. Biomechanics of Schlemm's canal endothelial cells: influence on F-actin architecture. Biophys J 2004; 87:2828-37. [PMID: 15454474].
9. Gabelt BT, Okka M, Dean TR, Kaufman PL. Aqueous humor dynamics in monkeys after topical R-DOI. Invest Ophthalmol Vis Sci 2005; 46:4691-6. [PMID: 16303966].
10. Green K. Free radicals and aging of anterior segment tissues of the eye: a hypothesis. Ophthalmic Res 1995; 27:Suppl 1143-9. [PMID: 8577453].
11. Lei Y, Stamer WD, Wu J, Sun X. Oxidative stress impact on barrier function of porcine angular aqueous plexus cell monolayers. Invest Ophthalmol Vis Sci 2013; 54:4827-35. [PMID: 23761078].
12. Lei Y, Stamer WD, Wu J, Sun X. Cell senescence reduced the mechanotransduction sensitivity of porcine angular aqueous plexus cells to elevation of pressure. Invest Ophthalmol Vis Sci 2014; 55:2324-8. [PMID: 24576879].
13. Sacca SC, Pascotto A, Camicione P, Capris P, Izzotti A. Oxidative DNA damage in the human trabecular meshwork: clinical correlation in patients with primary open-angle glaucoma. Arch Ophthalmol 2005; 123:458-63. .
14. Wang N, Chintala SK, Fini ME, Schuman JS. Activation of a tissue-specific stress response in the aqueous outflow pathway of the eye defines the glaucoma disease phenotype. Nat Med 2001; 7:304-9. [PMID: 11231628].
15. Izzotti A, Sacca SC, Cartiglia C, De Flora S. Oxidative deoxyribonucleic acid damage in the eyes of glaucoma patients. Am J Med 2003; 114:638-46. [PMID: 12798451].
16. Parikh P, Britt RD Jr, Manlove LJ, Wicher SA, Roesler A, Ravix J, Teske J, Thompson MA, Sieck GC, Kirkland JL, LeBrasseur N, Tschumperlin DJ, Pabelick CM, Prakash YS. Hyperoxia-induced Cellular Senescence in Fetal Airway Smooth Muscle Cells. Am J Respir Cell Mol Biol 2019; 61:51-60. [PMID: 30508396].
17. You K, Parikh P, Khandalavala K, Wicher S, Manlove LJ, Yang B, Roesler AM, Roos B, Teske JJ, Britt RD Jr, Pabelick CM, Prakash YS. Moderate hyperoxia induces senescence in developing human lung fibroblasts. Am J Physiol Lung Cell Mol Physiol 2019; 317:525-36. [PMID: 31411059].
18. Bu H, Wedel S, Cavinato M, Jansen-Durr P. MicroRNA Regulation of Oxidative Stress-Induced Cellular Senescence. Oxid Med Cell Longev 2017; 2017:2398696-[PMID: 28593022].
19. Beckman KB, Ames BN. The free radical theory of aging matures. Physiol Rev 1998; 78:547-81. [PMID: 9562038].
20. Liton PB, Lin Y, Luna C, Li G, Gonzalez P, Epstein DL. Cultured porcine trabecular meshwork cells display altered lysosomal function when subjected to chronic oxidative stress. Invest Ophthalmol Vis Sci 2008; 49:3961-9. [PMID: 18469195].
21. Campisi J, d'Adda di Fagagna F. Cellular senescence: when bad things happen to good cells. Nat Rev Mol Cell Biol 2007; 8:729-40. [PMID: 17667954].
22. Sitte N, Huber M, Grune T, Ladhoff A, Doecke WD, Von Zglinicki T, Davies KJ. Proteasome inhibition by lipofuscin/ceroid during postmitotic aging of fibroblasts. FASEB J 2000; 14:1490-8. [PMID: 10928983].
23. Terman A, Brunk UT. Ceroid/lipofuscin formation in cultured human fibroblasts: the role of oxidative stress and lysosomal proteolysis. Mech Ageing Dev 1998; 104:277-91. [PMID: 9818731].
24. Zheng L, Roberg K, Jerhammar F, Marcusson J, Terman A. Oxidative stress induces intralysosomal accumulation of Alzheimer amyloid beta-protein in cultured neuroblastoma cells. Ann N Y Acad Sci 2006; 1067:248-51. [PMID: 16803994].

25. Lei Y, Stamer WD, Wu J, Sun X. Oxidative Stress Impact on Barrier Function of Porcine Angular Aqueous Plexus Cell Monolayers. Invest Ophthalmol Vis Sci 2013; 54:4827-35. [PMID: 23761078].

26. Lei Y, Stamer WD, Wu J, Sun X. Endothelial nitric oxide synthase-related mechanotransduction changes in aged porcine angular aqueous plexus cells. Invest Ophthalmol Vis Sci 2014; 55:8402-8. [PMID: 25377220].

27. Bartel DP. MicroRNAs: target recognition and regulatory functions. Cell 2009; 136:215-33. [PMID: 19167326].

28. Lal A, Kim HH, Abdelmohsen K, Kuwano Y, Pullmann R Jr, Srikantan S, Subrahmanyam R, Martindale JL, Yang X, Ahmed F, Navarro F, Dykxhoorn D, Lieberman J, Gorospe M. p16(INK4a) translation suppressed by miR-24. PLoS One 2008; 3:e1864-[PMID: 18365017].

29. Wang Y, Scheiber MN, Neumann C, Calin GA, Zhou D. MicroRNA regulation of ionizing radiation-induced premature senescence. Int J Radiat Oncol Biol Phys 2011; 81:839-48. [PMID: 21093163].

30. Li G, Luna C, Qiu J, Epstein DL, Gonzalez P. Alterations in microRNA expression in stress-induced cellular senescence. Mech Ageing Dev 2009; 130:731-41. [PMID: 19782699].

31. Stellos K, Dimmeler S. Vascular microRNAs: from disease mechanisms to therapeutic targets. Circ Res 2014; 114:3-4. [PMID: 24385499].

32. Russo P, Fini M, Cesario A. Editorial: disease control and active and healthy ageing: new paradigms of therapeutic strategy. Curr Pharm Des 2014; 20:5919-20. [PMID: 24641221].

33. Maegdefessel L. The emerging role of microRNAs in cardiovascular disease. J Intern Med 2014; 276:633-44. [PMID: 25160930].

34. Zagryazhskaya A, Zhivotovsky B. miRNAs in lung cancer: a link to aging. Ageing Res Rev 2014; 17:54-67. [PMID: 24631464].

35. Tanaka Y, Tsuda S, Kunikata H, Sato J, Kokubun T, Yasuda M, Nishiguchi KM, Inada T, Nakazawa T. Profiles of extracellular miRNAs in the aqueous humor of glaucoma patients assessed with a microarray system. Sci Rep 2014; 4:5089-[PMID: 24867291].

36. Drewry MD, Challa P, Kuchtey JG, Navarro I, Helwa I, Hu Y, Mu H, Stamer WD, Kuchtey RW, Liu Y. Differentially expressed microRNAs in the aqueous humor of patients with exfoliation glaucoma or primary open-angle glaucoma. Hum Mol Genet 2018; 27:1263-75. [PMID: 29401312].

37. Jayaram H, Phillips JI, Lozano DC, Choe TE, Cepurna WO, Johnson EC, Morrison JC, Gattey DM, Saugstad JA, Keller KE. Comparison of MicroRNA Expression in Aqueous Humor of Normal and Primary Open-Angle Glaucoma Patients Using PCR Arrays: A Pilot Study. Invest Ophthalmol Vis Sci 2017; 58:2884-90. [PMID: 28586912].

38. Jayaram H, Cepurna WO, Johnson EC, Morrison JC. MicroRNA Expression in the Glaucomatous Retina. Invest Ophthalmol Vis Sci 2015; 56:7971-82. [PMID: 26720444].

39. Lei Y, Overby DR, Read AT, Stamer WD, Ethier CR. A new method for selection of angular aqueous plexus cells from porcine eyes: a model for Schlemm's canal endothelium. Invest Ophthalmol Vis Sci 2010; 51:5744-50. [PMID: 20554623].

40. Bolstad BM, Irizarry RA, Astrand M, Speed TP. A comparison of normalization methods for high density oligonucleotide array data based on variance and bias. Bioinformatics 2003; 19:185-93. [PMID: 12538238].

41. Pfaffl MW. A new mathematical model for relative quantification in real-time RT-PCR. Nucleic Acids Res 2001; 29:e45-[PMID: 11328886].

42. Zieske LR. A perspective on the use of iTRAQ reagent technology for protein complex and profiling studies. J Exp Bot 2006; 57:1501-8. [PMID: 16574745].

43. Gafken PR, Lampe PD. Methodologies for characterizing phosphoproteins by mass spectrometry. Cell Commun Adhes 2006; 13:249-62. [PMID: 17162667].

44. Cheng Y, Meng Q, Huang L, Shi X, Hou J, Li X, Liang J. iTRAQ-based quantitative proteomic analysis and bioinformatics study of proteins in retinoblastoma. Oncol Lett 2017; 14:8084-91. [PMID: 29344252].

45. Wu X, Pan X, Cao S, Xu F, Lan L, Zhang Y, Lian S, Yan M, Li A. iTRAQ-based quantitative proteomic analysis provides insights into strong broodiness in Muscovy duck (Cairina moschata) combined with metabolomics analysis. J Proteomics 2019; 204:103401-[PMID: 31152940].

46. Tatusov RL, Fedorova ND, Jackson JD, Jacobs AR, Kiryutin B, Koonin EV, Krylov DM, Mazumder R, Mekhedov SL, Nikolskaya AN, Rao BS, Smirnov S, Sverdlov AV, Vasudevan S, Wolf YI, Yin JJ, Natale DA. The COG database: an updated version includes eukaryotes. BMC Bioinformatics 2003; 4:41-[PMID: 12969510].

47. Li G, Luna C, Qiu J, Epstein DL, Gonzalez P. Modulation of inflammatory markers by miR-146a during replicative senescence in trabecular meshwork cells. Invest Ophthalmol Vis Sci 2010; 51:2976-85. [PMID: 20053980].

48. Gorospe M, Abdelmohsen K. MicroRegulators come of age in senescence. Trends in genetics TIG 2011; 27:233-41. [PMID: 21592610].

49. Meng X, Xue M, Xu P, Hu F, Sun B, Xiao Z. MicroRNA profiling analysis revealed different cellular senescence mechanisms in human mesenchymal stem cells derived from different origin. Genomics 2017; 109:147-57. [PMID: 28215993].

50. Bu H, Baraldo G, Lepperdinger G, Jansen-Durr P. mir-24 activity propagates stress-induced senescence by down regulating DNA topoisomerase 1. Exp Gerontol 2016; 75:48-52. [PMID: 26748253].

51. Mancini M, Saintigny G, Mahe C, Annicchiarico-Petruzzelli M, Melino G, Candi E. MicroRNA-152 and −181a participate in human dermal fibroblasts senescence acting on cell adhesion and remodeling of the extra-cellular matrix. Aging 2012; 4:843-53. [PMID: 23238588].

52. Rock K, Tigges J, Sass S, Schutze A, Florea AM, Fender AC, Theis FJ, Krutmann J, Boege F, Fritsche E, Reifenberger G, Fischer JW. miR-23a-3p causes cellular senescence by targeting hyaluronan synthase 2: possible implication for skin aging. J Invest Dermatol 2015; 135:369-77. [PMID: 25264594].

53. Hsu PY, Lin WY, Lin RT, Juo SH. MicroRNA let-7g inhibits angiotensin II-induced endothelial senescence via the LOX-1-independent mechanism. Int J Mol Med 2018; 41:2243-51. [PMID: 29393358].

54. Markopoulos GS, Roupakia E, Tokamani M, Vartholomatos G, Tzavaras T, Hatziapostolou M, Fackelmayer FO, Sandaltzopoulos R, Polytarchou C, Kolettas E. Senescence-associated microRNAs target cell cycle regulatory genes in normal human lung fibroblasts. Exp Gerontol 2017; 96:110-22. [PMID: 28658612].

55. Fu R, Yang P, Sajid A, Li Z, Avenanthramide A. Induces Cellular Senescence via miR-129–3p/Pirh2/p53 Signaling Pathway To Suppress Colon Cancer Growth. J Agric Food Chem 2019; 67:4808-16. [PMID: 30888162].

56. Liu X, Fu B, Chen D, Hong Q, Cui J, Li J, Bai X, Chen X. miR-184 and miR-150 promote renal glomerular mesangial cell aging by targeting Rab1a and Rab31. Exp Cell Res 2015; 336:192-203. [PMID: 26165933].

57. Overby DR, Zhou EH, Vargas-Pinto R, Pedrigi RM, Fuchshofer R, Braakman ST, Gupta R, Perkumas KM, Sherwood JM, Vahabikashi A, Dang Q, Kim JH, Ethier CR, Stamer WD, Fredberg JJ, Johnson M. Altered mechanobiology of Schlemm's canal endothelial cells in glaucoma. Proc Natl Acad Sci USA 2014; 111:13876-81. [PMID: 25201985].

58. Johnson M. 'What controls aqueous humour outflow resistance?'. Exp Eye Res 2006; 82:545-57. [PMID: 16386733].

59. Suh EJ, Remillard MY, Legesse-Miller A, Johnson EL, Lemons JM, Chapman TR, Forman JJ, Kojima M, Silberman ES, Coller HA. A microRNA network regulates proliferative timing and extracellular matrix synthesis during cellular quiescence in fibroblasts. Genome Biol 2012; 13:R121-[PMID: 23259597].

60. Yu G, Jia Z, Dou Z. miR-24–3p regulates bladder cancer cell proliferation, migration, invasion and autophagy by targeting DEDD. Oncol Rep 2017; 37:1123-31. [PMID: 28000900].

61. Wang H, Zhan Y, Jin J, Zhang C, Li W. MicroRNA-15b promotes proliferation and invasion of nonsmall cell lung carcinoma cells by directly targeting TIMP2. Oncol Rep 2017; 37:3305-12. [PMID: 28498424].

62. Kang L, Yang C, Yin H, Zhao K, Liu W, Hua W, Wang K, Song Y, Tu J, Li S, Luo R, Zhang Y. MicroRNA-15b silencing inhibits IL-1beta-induced extracellular matrix degradation by targeting SMAD3 in human nucleus pulposus cells. Biotechnol Lett 2017; 39:623-32. [PMID: 28039556].

63. Hernandez-Segura A, Nehme J, Demaria M. Hallmarks of Cellular Senescence. Trends Cell Biol 2018; 28:436-53. [PMID: 29477613].

64. Lopez-Otin C, Blasco MA, Partridge L, Serrano M, Kroemer G. The hallmarks of aging. Cell 2013; 153:1194-217. [PMID: 23746838].

65. Arthur WT, Petch LA, Burridge K. Integrin engagement suppresses RhoA activity via a c-Src-dependent mechanism. Curr Biol 2000; 10:719-22. [PMID: 10873807].

66. Huveneers S, Danen EH. Adhesion signaling - crosstalk between integrins, Src and Rho. J Cell Sci 2009; 122:1059-69. [PMID: 19339545].

67. Sumida GM, Stamer WD. Sphingosine-1-phosphate enhancement of cortical actomyosin organization in cultured human Schlemm's canal endothelial cell monolayers. Invest Ophthalmol Vis Sci 2010; 51:6633-8. [PMID: 20592229].

68. Tapon N, Hall A. Rho, Rac and Cdc42 GTPases regulate the organization of the actin cytoskeleton. Curr Opin Cell Biol 1997; 9:86-92. [PMID: 9013670].

69. Kameda T, Inoue T, Inatani M, Fujimoto T, Honjo M, Kasaoka N, Inoue-Mochita M, Yoshimura N, Tanihara H. The effect of Rho-associated protein kinase inhibitor on monkey Schlemm's canal endothelial cells. Invest Ophthalmol Vis Sci 2012; 53:3092-103. [PMID: 22491412].

70. Kaneko Y, Ohta M, Inoue T, Mizuno K, Isobe T, Tanabe S, Tanihara H. Effects of K-115 (Ripasudil), a novel ROCK inhibitor, on trabecular meshwork and Schlemm's canal endothelial cells. Sci Rep 2016; 6:19640-[PMID: 26782355].

71. Honjo M, Inatani M, Kido N, Sawamura T, Yue BY, Honda Y, Tanihara H. A myosin light chain kinase inhibitor, ML-9, lowers the intraocular pressure in rabbit eyes. Exp Eye Res 2002; 75:135-42. [PMID: 12137759].

72. Xia H, Nho RS, Kahm J, Kleidon J, Henke CA. Focal adhesion kinase is upstream of phosphatidylinositol 3-kinase/Akt in regulating fibroblast survival in response to contraction of type I collagen matrices via a beta 1 integrin viability signaling pathway. J Biol Chem 2004; 279:33024-34. [PMID: 15166238].

73. Lei Y, Zhang X, Song M, Wu J, Sun X. Aqueous Humor Outflow Physiology in NOS3 Knockout Mice. Invest Ophthalmol Vis Sci 2015; 56:4891-8. [PMID: 26225628].

74. Chang JY, Stamer WD, Bertrand J, Read AT, Marando CM, Ethier CR, Overby DR. Role of nitric oxide in murine conventional outflow physiology. Am J Physiol Cell Physiol 2015; 309:C205-14. [PMID: 26040898].

75. Garcia GA, Ngai P, Mosaed S, Lin KY. Critical evaluation of latanoprostene bunod in the treatment of glaucoma. Clin Ophthalmol 2016; 10:2035-50. [PMID: 27799730].

76. Okamoto T, Kawamoto E, Takagi Y, Akita N, Hayashi T, Park EJ, Suzuki K, Shimaoka M. Gap junction-mediated regulation of endothelial cellular stiffness. Sci Rep 2017; 7:6134-[PMID: 28733642].

77. Mikoshiba K. IP3 receptor/Ca2+ channel: from discovery to new signaling concepts. J Neurochem 2007; 102:1426-46. [PMID: 17697045].

78. Orellana JA, Sanchez HA, Schalper KA, Figueroa V, Saez JC. Regulation of intercellular calcium signaling through calcium

interactions with connexin-based channels. Adv Exp Med Biol 2012; 740:777-94. [PMID: 22453969].

79. Patel LS, Mitchell CK, Dubinsky WP, O'Brien J. Regulation of gap junction coupling through the neuronal connexin Cx35 by nitric oxide and cGMP. Cell Commun Adhes 2006; 13:41-54. [PMID: 16613779].

80. Harburger DS, Calderwood DA. Integrin signalling at a glance. J Cell Sci 2009; 122:159-63. [PMID: 19118207].

81. Torgler CN, Narasimha M, Knox AL, Zervas CG, Vernon MC, Brown NH. Tensin stabilizes integrin adhesive contacts in Drosophila. Dev Cell 2004; 6:357-69. [PMID: 15030759].

82. Theodosiou M, Widmaier M, Bottcher RT, Rognoni E, Veelders M, Bharadwaj M, Lambacher A, Austen K, Muller DJ, Zent R, Fassler R. Kindlin-2 cooperates with talin to activate integrins and induces cell spreading by directly binding paxillin. eLife 2016; 5:e10130-[PMID: 26821125].

83. Mitra SK, Schlaepfer DD. Integrin-regulated FAK-Src signaling in normal and cancer cells. Curr Opin Cell Biol 2006; 18:516-23. [PMID: 16919435].

84. Santas AJ, Bahler C, Peterson JA, Filla MS, Kaufman PL, Tamm ER, Johnson DH, Peters DM. Effect of heparin II domain of fibronectin on aqueous outflow in cultured anterior segments of human eyes. Invest Ophthalmol Vis Sci 2003; 44:4796-804. [PMID: 14578401].

Articles are provided courtesy of Emory University and the Zhongshan Ophthalmic Center, Sun Yat-sen University, P.R. China. The print version of this article was created on 25 February 2020. This reflects all typographical corrections and errata to the article through that date. Details of any changes may be found in the online version of the article.